TECHNICAL PAPER

CrossMark

The effect of purge gas condition on the amount of ferrite in tubular AISI 304 stainless steel during welding

Laécio G. Galdino[1,4] · Samuel F. Rodrigues[2] · Clodualdo Aranas Jr.[3] · Gedeon S. Reis[2] · Valtair A. Ferraresi[4]

Abstract

The primary objective of the present work is to evaluate the influence of various commercial gases on the microstructure of tubular AISI 304 austenitic stainless during welding. This was carried out using CO_2, Ar, N_2, Ar + 25%CO_2 and Ar + 2%O_2 gases, which are common inert gases or mixture specified in numerous technical standards associated with welding. These five gases were evaluated using flow rate range of 6–18 L/min. Different welding speeds, wire feed speeds, shield gases (Ar + 2% O_2), distance nozzle contact pieces, voltages and currents were employed to validate the present observations. The microstructures of the samples were evaluated along the cross section of the face of the weld using optical microscopy. The samples were further analyzed by means of magnetic testing, which could provide information related to the evolution of ferrite. The estimated phase fractions were then compared to the predictions provided by the Welding Research Council (WRC-92) diagram. The optical microscopy images showed small microstructural variations between the samples with different gas purge conditions, even when using the maximum gas flow rate. However, these observations were inconsistent with the magnetic response of the material, which provided significant differences in the phase fractions between the face and the root of the weld. The discrepancies between these two methods were analyzed to evaluate the phases and consistently track the phase fractions after welding.

Keywords Welding · Ferrite content · Austenitic stainless steel · Gas purge

1 Introduction

Optimization of industrial processes is one of the key factors in maintaining and improving the quality of numerous industry products. In metallic materials, there is a constant search for improvement in its mechanical

✉ Samuel F. Rodrigues
samuel.filgueiras@ifma.edu.br

1 Department of Professional Education, Federal Institute of Education, Science and Technology of Maranhão, Imperatriz, MA, Brazil

2 PPGEM, Department of Mechanical and Materials, Federal Institute of Education, Science and Technology of Maranhão, São Luís, MA, Brazil

3 Department of Mechanical Engineering, University of New Brunswick, Fredericton, NB, Canada

4 Laprosolda – Centre for Research and Development of Welding Processes, School of Mechanical Engineering, Federal University of Uberlandia, Uberlândia, MG, Brazil

properties and corrosion resistance [1]. This is also similar in the field of welding of metals [2–6]. The behavior of materials during welding can be significantly affected by modifications in the fabrication processes. However, these changes can result in sudden fluctuation in the cost and quality, which identifies the competitiveness of the product. In this line of thought, it is the objective of the present study to evaluate the properties and behavior of the face and root of a weld while protected with various gas purging conditions. This work will benefit the continuously increasing demand of these types of studies in the welding industry in the past several years [2, 3].

During welding of stainless steel tubular components, it is a common practice to use gas purging to protect the weld during melting and solidification processes [3, 6]. The presence of gas minimizes the high-temperature reaction of the weld with air and other atmospheric impurities, which affects the quality of the weld. Moreover, formation of phases such as δ-ferrite and its morphology must be controlled, depending on the application of stainless steels [7, 8]. Note that the properties of the tubular pipe, with

special attention to the weld, are dependent on the type of gas, the location of the gas outlet, the size of exhaust system and gas pressure since these parameters affect the effectivity of gas purging [9]. The root of the weld is a critical part of the tubular joint due to various reactions when heat is applied during welding [10]. For instance, Wang et al. [11] demonstrated the effects of different processing parameters on the microstructural growth kinetics in a stainless steel weld, which could alter its mechanical properties. Other studies focused on finding cheaper alternative protective gas such as nitrogen, which can also be mixed with argon, helium and hydrogen. These gas mixtures are proven to effectively protect and improve the properties of materials as shown by Westin et al. [12]. In their work, they demonstrated that small additions of gas mixtures can effectively suppress oxidation in steels and can affect the precipitation of Cr_2N in the weld. These precipitates are known to increase the corrosion resistance of steels. Therefore, the optimization of gas purging condition during welding can be an effective tool to improve the corrosion properties of the weld [13, 14].

The primary objective of this work is to evaluate the effect of purging gas condition on the amount of ferrite in austenitic stainless steel pipes by using various gases and gas mixtures during welding. This was obtained using microstructural analysis, magnetic response measurement of the samples using ferritescope and evaluation of Welding Research Council (WRC-92) diagram [15]. The present results are expected to maximize the mechanical and physical properties of the pipe joints during welding.

2 Experimental procedures

2.1 Materials

The test tubes (TT), which act as a base metal (BM), were made of AISI 304 austenitic stainless steel. The tubes have diameters and wall thicknesses of 60 and 2.77 mm, respectively. The electrode wire (EW) is made of ER 208LSi alloy and has a diameter of 1.2 mm. The chemical compositions of BM and EW are listed in Table 1.

Table 1 Nominal chemical composition of the AISI 304 austenitic stainless steel tube (BM) and ER 308LSi electrode wire (AE)

Materials	Chemical elements and limit concentration (%)							
	C	Mn	Si	Cr	Ni	Cu	Mo	N
BM	0.048	1.19	0.370	18	8	0.1207	0.083	–
EW	0.024	1.8	0.9	20	10.5	–	0.028	0.05

A commercial mixture of Ar + 2%O_2 was used as a protective gas atmosphere with a constant flow rate of 15 L/min. For gas purging, different gases such as CO_2, Ar, N_2, Ar + 25%CO_2 and Ar + 2%O_2 were employed with flow rates of 6, 12 and 18 L/min. Variation in the type of gas was employed to determine the reaction of the microstructure upon application of each type of gas. The flow rate was monitored by using a digital flow meter incorporated into the purge system device.

2.2 Welding device and gas purging system

The welding of the test tubes was restricted to position 1G, with the torch remained fixed and vertically aligned to the welded joint. The tube can freely rotate by means of equipment developed for such purpose (Fig. 1). In the injection of the gas purge to the system, a device was developed that could be coupled to the rotation system of the test tubes, so as to comply with the procedures defined in AWS D10.4 [16]. The procedure for purge cycle consists of pre-purge cycle, which is performed by purging out the ambient air and by maintaining an adequate flow of gas to protect the joint and other parts of the components that have to be welded (Fig. 1a–e). The element (e) in Fig. 1 highlights the diffuser device for the gas purging developed technically according to the characteristics of the equipment and test tubes involved. This aimed to keep the purge gas directly in the root throughout the welding.

The test tubes (TT) were made from two symmetrical tubes, as shown in Fig. 2, with a bevel angle of 45°, width of 35 mm and nose height of 0.5 mm. In order to avoid overlapping effects of the injected gases, purge exhaust holes were included at the end of the TT, equidistant with respect to the weld. Modifications in the manufacturing conditions of TT were made to avoid overpressure effects,
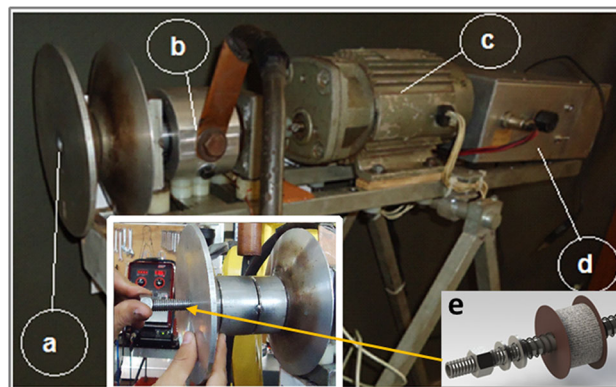

Fig. 1 Device for fixing and rotating the test tubes: **a** conical disks for securing tubular parts with central hole for fixing device, **b** aluminum tank with mercury connected to the earth cable, **c** electric motor with transmission for system rotation, **d** motor control potentiometer, **e** detachment from diffuse device to the purge

Fig. 2 a A diagram of the test tube with dimensions (TT) and **b** the location of the exhaust holes
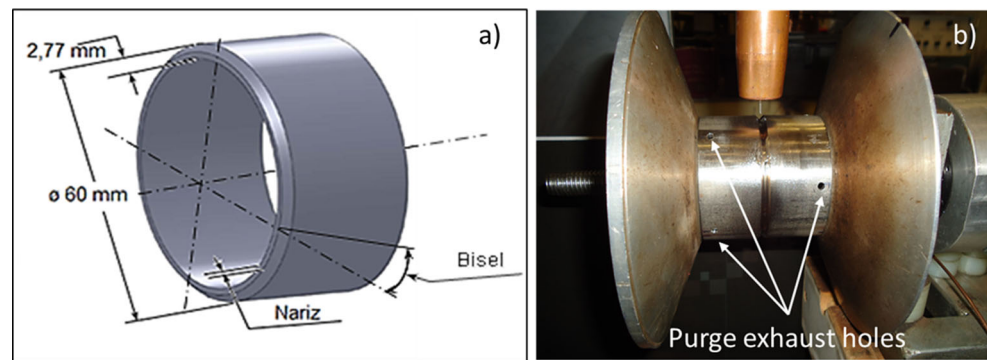
in accordance with the quality maintenance practices recommended by Fletcher [2] and Ma et al. [9] for welds in systems with purge system.

2.3 Welding parameters

The welds were made by gas metal arc welding (GMAW) using STT® technology and automatic feeder. The torch used in all tests had water cooling with maximum current capacity of up to 450 A during welding. Using the program 126 for stainless steel welding, the electronic source itself was limited to the settings of the base current—B_c, peak current—P_c, feed rate—F_r, "tail-out", pre-flow time and post-flow time.

A robotic mechanical arm performed the positioning and adjustment of the torch in relation to the welded joint to ensure the reproducibility of dimensional variables (i.e., 1G position) [17] that could influence the welding process.

The parameters applied in the definite tests were: base current—B_c = 160 A; peak current—P_c = 300 A; electrode wire feed velocity—F_r = 4.54 m/min; distance contact part nozzle—DCPN = 12 mm; and tangential welding velocity—T_{wv} = 50.1 cm/min.

2.4 Metallography and magnetic testing

The metallographic analysis of selected samples was conducted according to the procedure defined in the ASM International Handbook [18] and ASTM-E407-07 standard [19]. The samples were cut, mounted and polished, followed by etching using Villela's reagent to reveal the microstructure. The microstructural observation of fusion zone (FZ) with various purging conditions was made using a light microscope with magnifications from 200 × to 1000 ×. The area of interest for this analysis is highlighted in Fig. 3.

The analysis of ferrite content was performed by means of a portable ferritescope. The procedures adopted for this work are described in Fig. 4. The schematic diagram of the magnetic measurement method performed on the face and
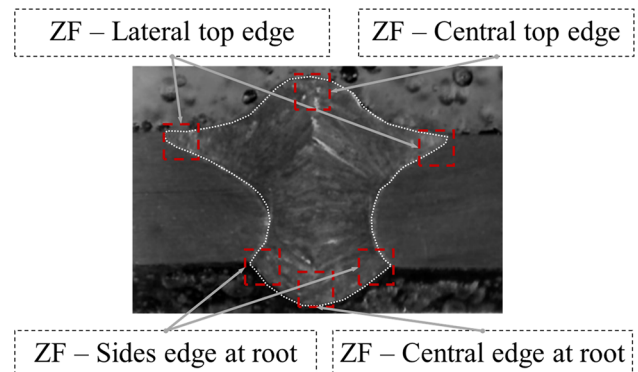

Fig. 3 Schematic diagram of the area of interest in the fusion zone (FZ)

root of the weld is shown in Fig. 4a. On the other hand, the magnetic measurements in the cross section of the weld are displayed in Fig. 4b. Note that the microstructures were analyzed in the cross section of the weld. Both measurements were performed perpendicular to the area of interest.

3 Results and discussion

3.1 Analysis of WRC diagram

By using the WRC diagram, the amount of phases in the welded joint can be easily predicted which can provide preliminary data for analysis. Once the dilution data were obtained by means of macrographs of samples, A, B and C as shown in Fig. 4b, the data of Table 2 are organized.

According to the WRC diagram (Fig. 5), the Fusion Zone (FZ) even with a variation around 4% will not have a great difference in terms of its microstructure. Basically, it will be composed of ferrite + austenite with a quantity of ferrite around 6%.

The dilution data associated with each test condition are shown in Fig. 6. The average variation indicated a possible drop for the less oxidizing purge gases or mixtures. The most oxidizing mixture (TT14 to TT16) with Ar + 2% of

Fig. 4 Schematic diagram for the analysis of ferrite content in the: **a** cord surfaces (face and root) and **b** cross section of the weld
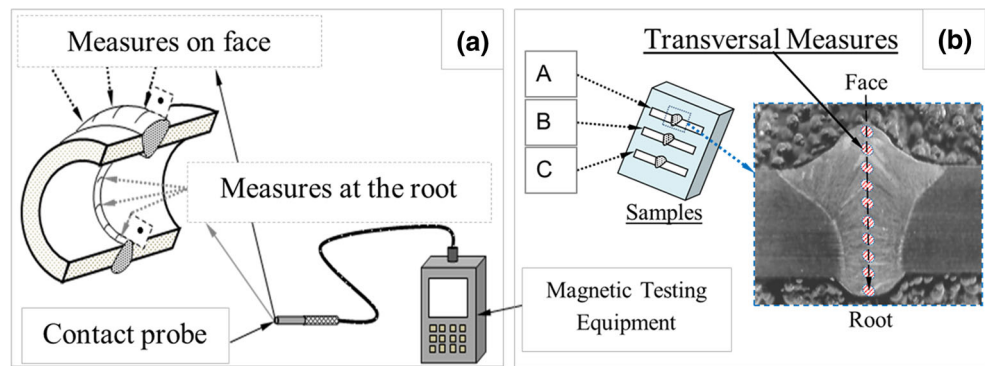

Table 2 WRC correlations based on the values of Table 1 and dilution (δ)

Correlations	MB	EW
$Ni_{equivalent} = Ni + 35C + 20N + 0.25\ Cu =$	9.71	12.34
$Cr_{equivalent} = \%Cr + \%Mo + 0.7 \times \%\ Nb =$	18.08	20.03

Dilution (δ) based on the sections: *A*, *B* and *C*

Samples	A	B	C	Average	SD
TT1—no purge gas	32.00	29.90	32.98	31.63	1.57
TT2—CO_2 at 6 L/min	29.31	30.59	30.92	30.27	0.85
TT3—CO_2 at 12 L/min	31.4	31.99	37.13	33.51	3.15
TT4—CO_2 at 18 L/min	29.52	25.84	31.93	29.10	3.07
TT5—Ar at 6 L/min	34.61	32.32	32.86	33.26	1.20
TT6—Ar at 12 L/min	32.58	35.36	30.88	32.94	2.26
TT7—Ar at 18 L/min	34.14	30.35	31.71	32.07	1.92
TT8—N_2 at 6 L/min	31.87	30.52	31.33	31.24	0.68
TT9—N_2 at 12 L/min	30.52	32.42	31.58	31.51	0.95
TT10—N_2 at 18 L/min	28.3	28.96	27.69	28.32	0.64
TT11—Ar + 25%CO_2 at 6 L/min	27.78	29.96	31.59	29.78	1.91
TT12—Ar + 25%CO_2 at 12 L/min	29.42	30.45	28.63	29.50	0.91
TT13—Ar + 25%CO_2 at 18 L/min	31.69	26.81	28.89	29.13	2.45
TT14—Ar + 2%O_2 at 6 L/min	29.58	26.45	31.60	29.21	2.59
TT15—Ar + 2%O_2 at 12 L/min	32.58	31.57	34.81	32.99	1.66
TT16—Ar + 2%O_2 at 18 L/min	33.36	34.11	34.18	33.88	0.45

TT test tube

O_2 developed higher levels of dilution as the flow rate was increased.

3.2 Metallographic analysis

The metallographic evaluation by means of optical microscopy was conducted using magnifications of 50 ×

and 1000 ×. In the search for the largest possible deviation, the purge conditions were taken where the flow rate was maintained at 18 L/min and these were compared to the reference condition without purge gas at the root. Figure 7 shows microstructures with a magnification of 50 ×. In this magnification, it is possible to observe the transversal behavior in a still macroscale aspect of the molten zone. In the upper part of the cord, the same gas condition was maintained by using as protection gas Ar + 2%O_2. It can be seen that along the edges of the molten zone, a practically homogeneous aspect of the dark regions, which characterizes the ferrite shafts, is visible. This was analyzed in larger magnifications below.

Figure 8 represents the reference condition, which corresponds to the retained sample of TT1 without application of purge gas. Due to the position of the regions selected for microanalyses, only very slight distortion due to the location at the edge of the sample is very common. However, it can be clearly observed that, in the TT1 sample, the 1000 × magnifications show little difference between the microstructures formed in the FZ.

The microstructures formed at the upper edge of the welded bead in the FZ of TT1 (Fig. 8) basically consist of austenite with ferrite shafts distributed in a spine and/or laminar form. In the root, the microstructure is similar, without different microstructural formations. The morphological orientation of the ferrite shafts on the lateral images of both the upper and lower root regions follows the columnar formation behavior, typical for the welded joint zones even in this cut position of the sample, which is most likely aligned in the direction of heat extraction. In the center of the optical images, between the upper and root edge, the cross sectional position of the samples reveals the interlacing region of the columnar grains from the sides. There are no significant expansions or dimensional reductions highlighting large differences between the upper and lower edges in the root, or any indications of a possible enlargement or reduction of the austenitic field.

In Fig. 9, the micrograph of the sample transverse to the CO_2-purged string at a flow rate of 18 L/min is shown. The

Fig. 5 Representation in the WRC-92 diagram: base metal, electrode wire-EW (308LSi) and FZ region as dilutions
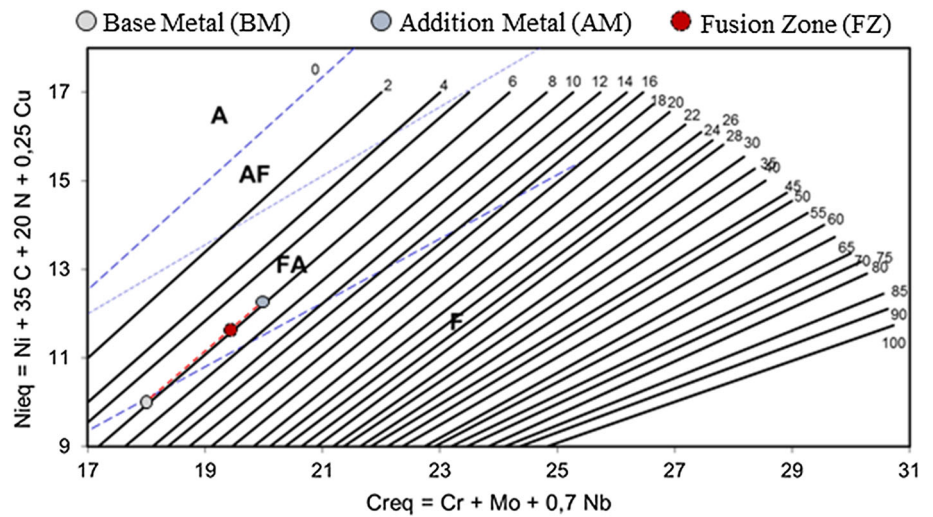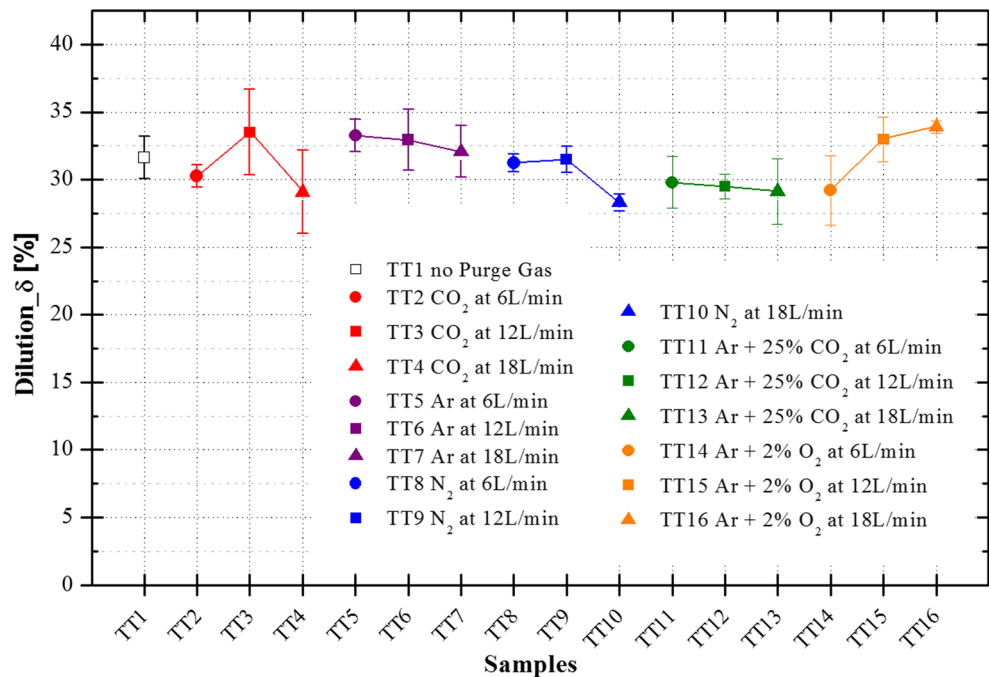

Fig. 6 Behavior of the dilution between the purging conditions

presence of ferrite shafts is distributed in a very homogeneous manner, both at the upper border of the FZ and at the root. Similar to the reference condition, without the gas purging, it is not possible to distinguish significant changes in the austenitic and ferritic phases either within the regions of this same sample or by comparing with the reference condition TT1. Even the presence of carbon during gas purging (in the form of carbon dioxide), which can contribute strongly to the austenite formation [20], did not produce observable changes in the microstructure.

In Fig. 10, the micrograph of the FZ purged with the inert gas argon is shown. The microstructural behavior of this analyzed sample did not present distinct modifications in relation to the other cases. In the images of the upper border of the FZ compared to the edge of the root, the behavior of the austenitic phase remained homogeneous and distributed similarl to the previous conditions analyzed.

The images of Fig. 11 are associated with samples purged with nitrogen. This chemical element, when added to the shielding gas in the welding process, allows high influence on the austenitic field expansion. However, even at a flow rate of 18 L/min as applied to the test condition defined as TT10, it did not present distinguishable expansions in the cutting section of the sample analyzed metallographically. However, the average values of ferrite, analyzed in this test tube by the magnetic field test, showed
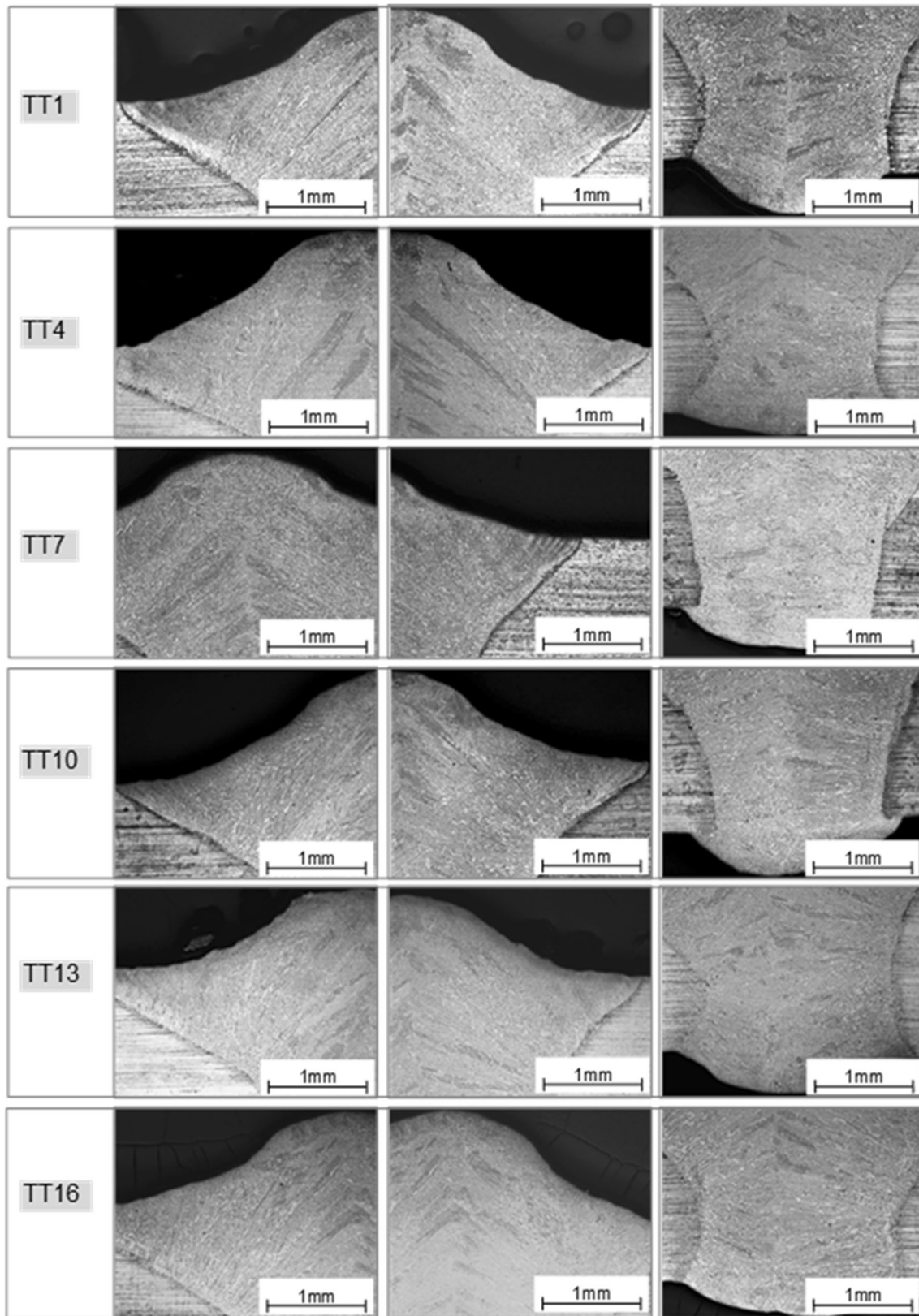
Fig. 7 Cross section metallographs of the test tubes: TT1—no purge gas; TT4—CO$_2$ at 18 L/min; TT7—Ar at 18 L/min; TT10—N$_2$ at 18 L/min; TT13—Ar + 25%CO$_2$ at 18 L/min; and TT16— Ar + 2%O$_2$ at 18 L/min; highlighting the top and the root of the cord with × 50 magnification

Fig. 8 Micrographs of the edges in the FZ with a magnification of × 1000: TT1—without application of purging gas
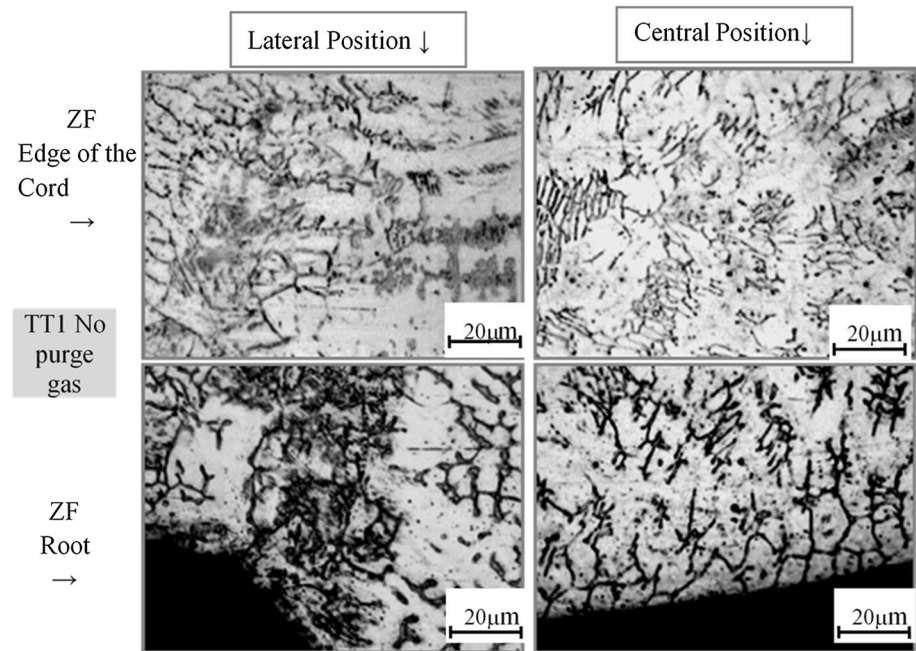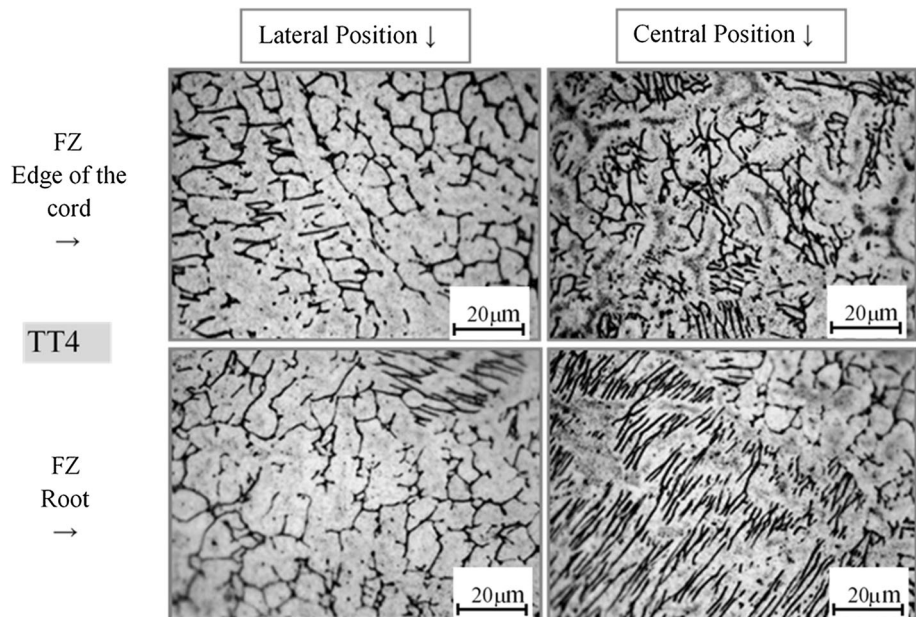

Fig. 9 Micrographs with × 1000 magnification: TT4—purge with CO_2 at 18 L/min

that even though the flow rate varied in 6, 12 and 18 L/min, it remained practically the same.

The application of gas purging using a mixture containing 25% CO_2 and 75% argon, see Fig. 12, with a higher flow rate of 18 L/min, also did not bring different variations in the type or behavior of the microstructures in the metallographic images of this weld sample.

Finally, a gas purge at the root employing Ar + 2% O_2 gas mixture at the same flow rate of 18 L/min was applied. The metallographic result is showed in Fig. 13.

As can be seen in Fig. 13, similar to the images of the samples under the previous conditions, no new or significant changes were detected metallographically. It is possible that the differentiated changes in the dilution behavior (due to the shape of the welded joint) contribute to the changes in the ferrite content, which will be further analyzed by means of the magnetic testing in the next section below.

From the comparisons between the micrographs of all the purging conditions used here, it is observed that the formation of spiral and lace ferrite has similar proportions.

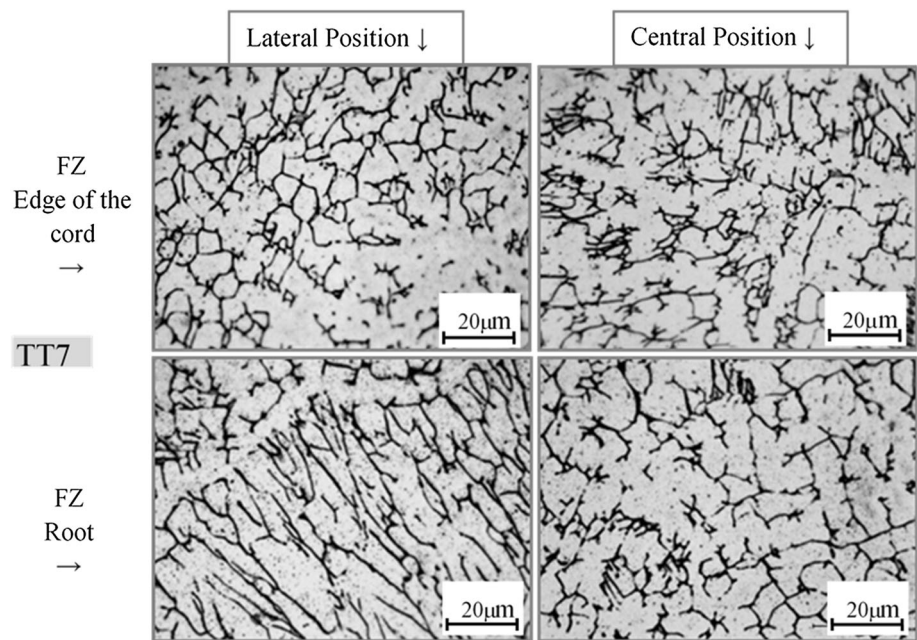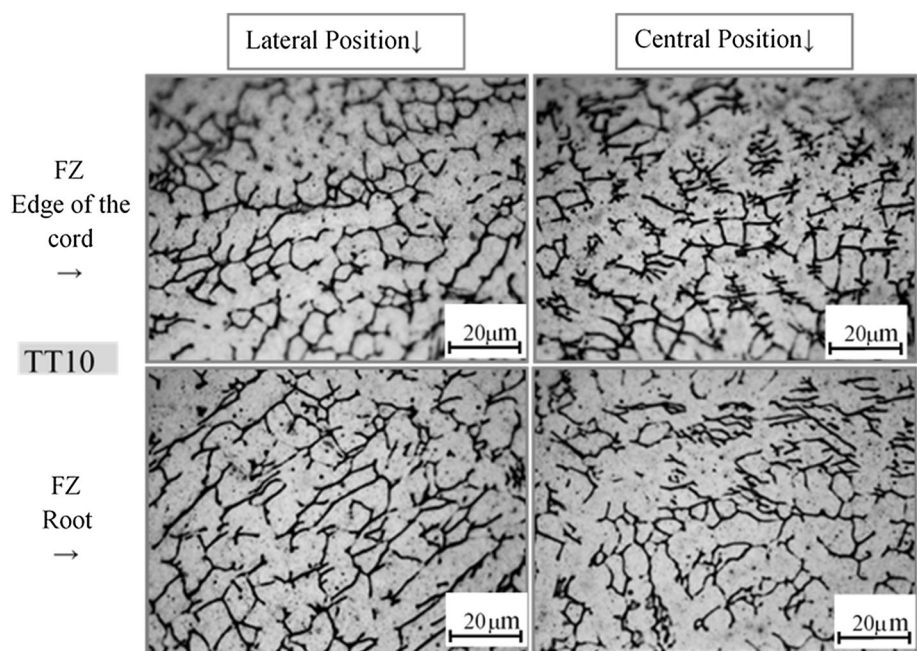**Fig. 10** Micrographs with a magnification of × 1000: TT7—purged with Ar at 18 L/min

Fig. 11 Micrographs with magnification of × 1000: TT10—purged with N_2 at 18 L/min

As shown by Inoue et al. [21], it is difficult to establish a comparative pattern between the phases of these ferritic microstructures.

The austenitic microstructure also did not present significant visual alterations that justified a more detailed dimensional analysis. The testing conditions imposed here displayed a homogeneous distribution of microstructure.

3.3 Analysis of the ferrite by magnetic test

The ferrite content was measured using a ferritescope at the face of the weld bead, root surface and along the vertical-transverse profile. Note that the magnetic response of the material can accurately characterize the behavior of the ferritic phase.

The mean values and standard deviations of the ferrite content are listed in Table 3. According to the analysis scheme presented in Fig. 4a, the values listed in Table 3

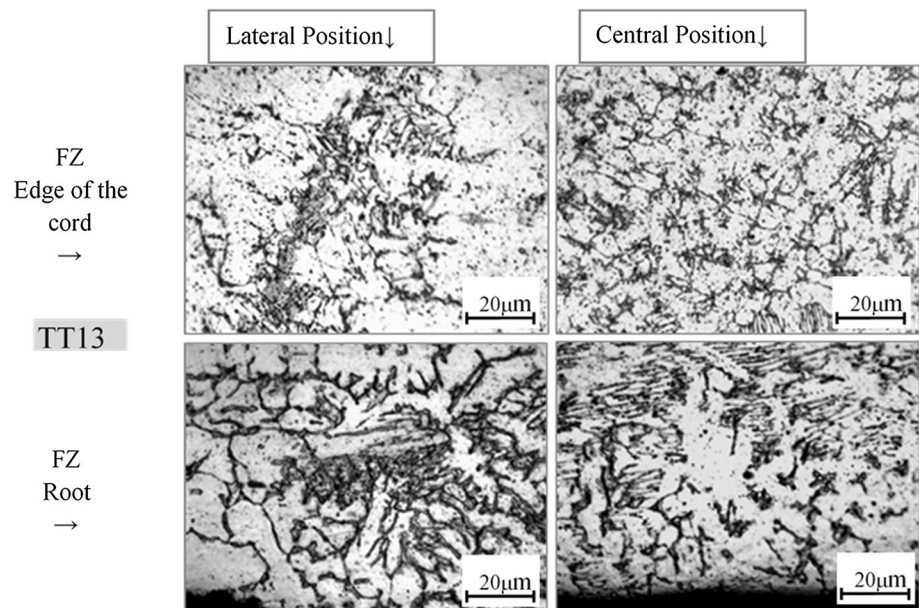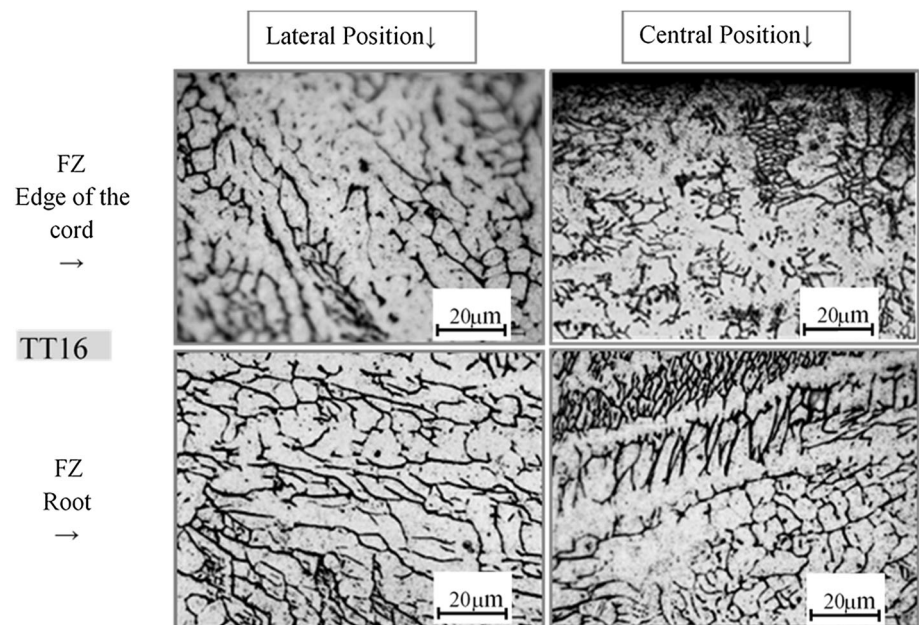**Fig. 12** Micrographs with × 1000 magnification: TT13—purged with Ar + 25%CO₂ at 18 L/min

Fig. 13 Micrographs with magnification of × 1000: TT16—purged with Ar + 2% O₂ at 18 L/min

are collected in the face of the cord and the root, with eight measurements in every test condition.

In Fig. 14, it is possible to visualize the behavior of the ferrite content in the face of the cord and root developed in the melted zone of various TTs. It can be observed that there is a more distinct variation in terms of mean values of ferrite content between the samples with different gas purging conditions. Such behavior is not evident in the metallographic investigation.

In the graphs of Fig. 15, the analysis of ferrite contents using different purge gases is presented. However, in order to better evaluate the behavior toward the formation of the

ferrite in the FZ region, the values measured in the central position of the samples A, B and C (sectioned in the transverse-vertical position of the cord) are considered, as shown earlier in Fig. 4b.

The ferrite content in the samples with different gas purging conditions is within the expected range of values based on the analysis of the WRC-92 diagram in Sect. 3.1. This is clearly seen in Fig. 15. Note that these plots are separated according to gas purging conditions. Practically, all the conditions presented a discrepancy when evaluating the mean value of ferrite content, and more specifically, a difference in ferrite content was observed between the root

Table 3 Data measured by magnetic test (ferrite content—%)

Samples	Positions of measures in the FZ					
	Weld face		Center between face and root (cross section)		Root surface	
	Average	SD	Average	SD	Average	SD
MB	0.90	0.12	1.73	0.21	0.52	0.08
TT1—no purge gas	5.19	0.38	7.24	0.28	5.53	0.22
TT2—CO_2 at 6 L/min	5.32	0.41	7.70	0.37	5.73	0.40
TT3—CO_2 at 12 L/min	5.14	0.31	7.36	0.05	5.26	0.30
TT4—CO_2 at 18 L/min	5.18	0.29	7.49	0.15	6.21	0.45
TT5—Ar at 6 L/min	5.21	0.38	7.41	0.16	5.88	0.32
TT6—Ar at 12 L/min	5.27	0.35	7.53	0.10	5.73	0.58
TT7—Ar at 18 L/min	5.04	0.37	7.05	0.18	6.09	0.48
TT8—N_2 at 6 L/min	5.00	0.32	7.39	0.22	5.58	0.32
TT9—N_2 at 12 L/min	5.03	0.26	7.41	0.12	5.31	0.36
TT10—N_2 at 18 L/min	5.10	0.31	7.13	0.10	5.34	0.40
TT11—Ar + 25%CO_2 at 6 L/min	4.98	0.27	7.14	0.05	5.63	0.56
TT12—Ar + 25%CO_2 at 12 L/min	5.45	0.38	7.33	0.14	6.24	0.46
TT13—Ar + 25%CO_2 at 18 L/min	5.51	0.35	7.64	0.18	6.48	0.22
TT14—Ar + 2%O_2 at 6 L/min	5.02	0.33	7.36	0.18	5.55	0.41
TT15—Ar + 2%O_2 at 12 L/min	5.15	0.22	7.43	0.23	6.08	0.43
TT16—Ar + 2%O_2 at 18 L/min	5.13	0.22	7.69	0.06	5.96	0.26

MB base metal, *TT* test tube

and the face of the cord. This observation is more obvious in the gas or mixtures of a more reactive chemical. However, within the evaluation of the respective deviant patterns, all samples showed similar profiles.

Concerning the interference in the formation of the ferritic phase, the data in Fig. 15 indicate that the simple use of the gas in the purging system minimized their degradation, specifically when the samples are compared to the condition without gas purging. This effect was most evident when the purge flow rate was increased, except for the N_2 gas.

An unusual phenomenon in the data of Fig. 15 is evident due to the higher ferrite profile analyzed in the center of the cords of the different samples tested. In order to better understand this behavior, TT4 samples (with CO_2-based purge at the maximum test flow, 18 L/min) were taken and a more detailed cross-vertical profile analysis was performed in the central line (Fig. 4b). The result of this analysis is shown in Table 4. The respective graph of these values reveals the profile of the ferrite content (Fig. 16) reaching a maximum peak close to the center of the cord.

Figure 16 illustrates the dependence of the ferrite content along the vertical center line in the FZ. The measurements were performed on the surfaces of the samples shown in Fig. 4b and are depicted in Table 4. The column with mean values is the result of the measurements of the sample cuts A, B and C according to the analyzed TT.

In Fig. 16, it is possible to clearly understand the variation in ferrite content observed as compared to the predictions of WRC-92 diagram. The oxidation of the chemical elements in the melting pool may be one of the main reasons for this behavior. In the melting pool, the thermal effects from the electric arc create more favorable conditions to the gas protection of the torch, resulting in greater level of interaction with the chemical elements that will solidify in the proximities of the face of the cord. Researchers such as Inoue et al. [21], Liao et al. [22] and Filho et al. [23] have found in their studies that the gas mixture Ar + 2% CO_2, when used as protection in the torch, can interfere with the chromium composition of the sample and reduce the ferrite content. However, in the root, given the lower thermal level and physical–chemical effects of solidification and cooling of the FZ, due to the welding conditions and materials used, the deleterious effects on the level of the ferrite content were lower than those on the face.

4 Conclusion

Based on the present work, the following can be concluded:

1. The influence of different gas purging conditions on the microstructure of AISI 304 stainless steel joints

Fig. 14 Behavior of ferrite content in the fusion zone (FZ): face and root of the strands
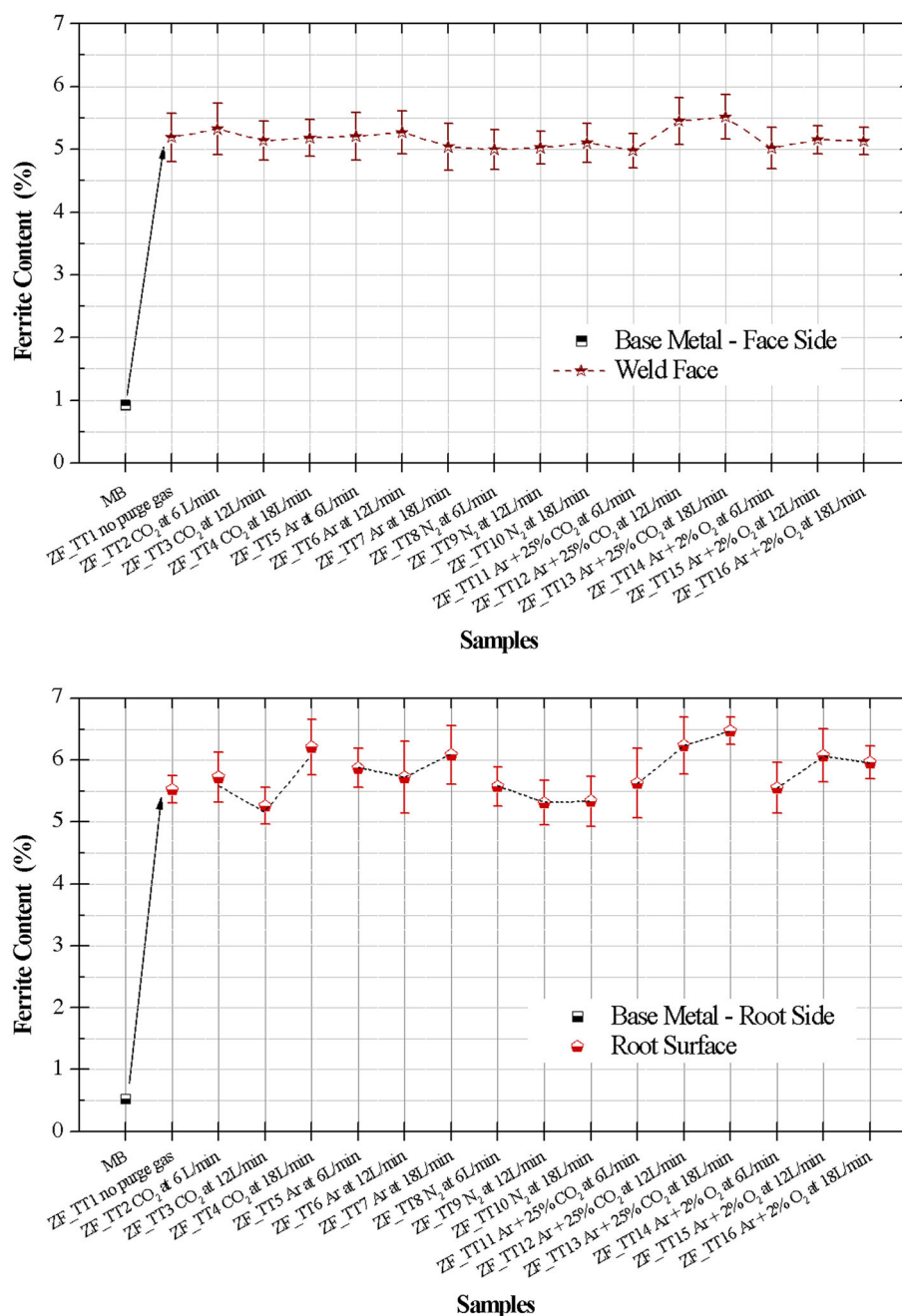
during pipe welding was evaluated. Although the optical microstructures did not provide visual variations in ferrite content, the magnetic testing by means of ferritescope was able to accurately detect the differences in ferrite content of samples with different gas purging conditions.

2. The variation in dilution between different gas purging conditions provided a lower level of change when compared to the effect of additional protective gas $Ar + 2\%O_2$ in the torch.

3. The use of shielding gas in the torch $(Ar + 2\%O_2)$ reduces the levels of ferritic phase formation in the face of the weld. The gas purging using different gases such as CO_2, air and N_2 or mixtures such as $Ar + 25\%CO_2$ and $Ar + 2\%O_2$, even those with alpha elements, will not expand the ferrite content in the root of the weld. This will not also maintain the ferrite content across the center of the cord.

4. The use of the above-mentioned purge gases can minimize the degradation of materials compared to welding without gas purging. This effect was more

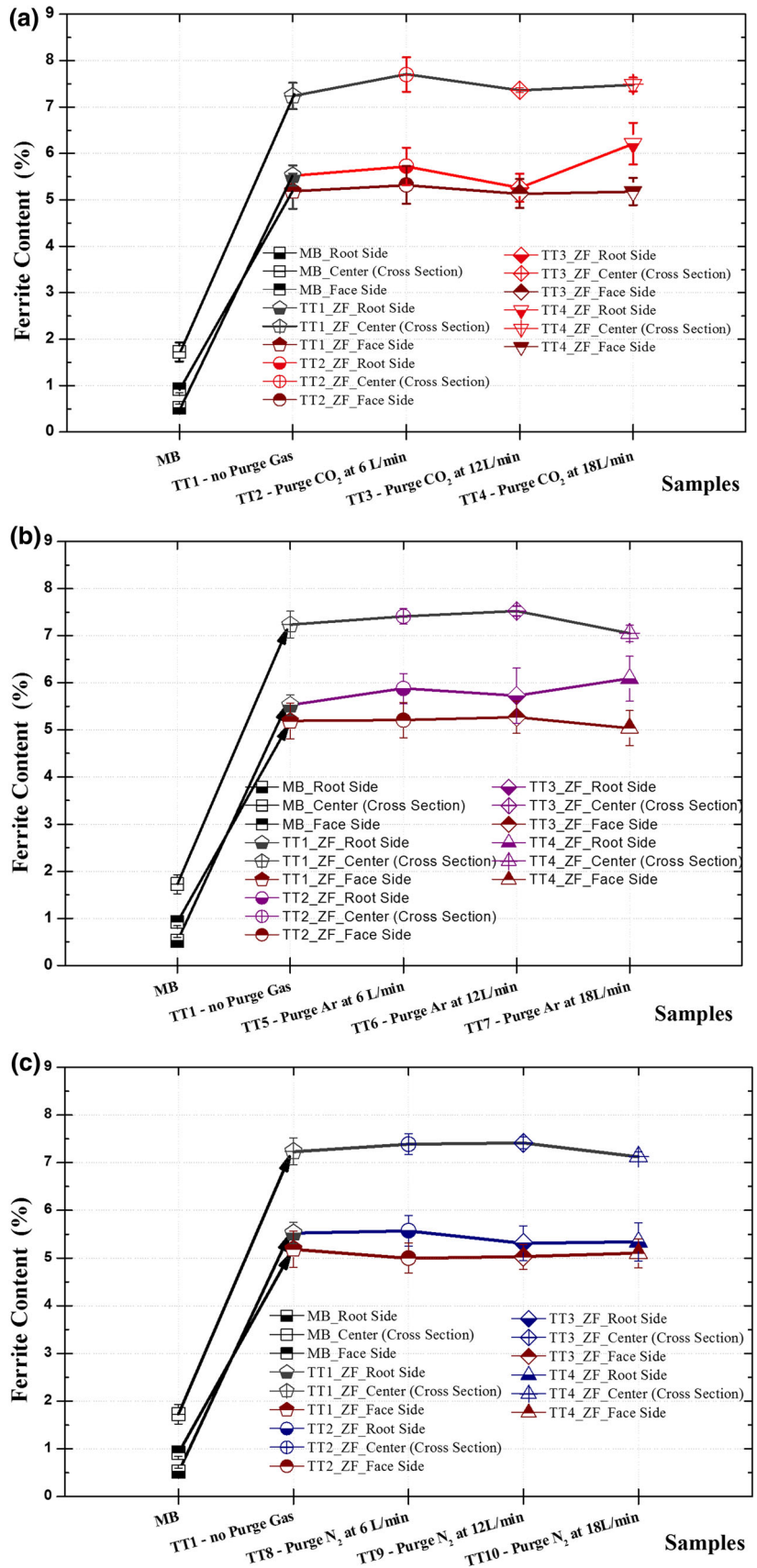**Fig. 15** Ferrite content by purge condition and FZ measurements in the condition: face–center–root

Fig. 15 continued

(d)

Legend:
- MB_Root Side
- MB_Center (Cross Section)
- MB_Face Side
- TT1_ZF_Root Side
- TT1_ZF_Center (Cross Section)
- TT1_ZF_Face Side
- TT2_ZF_Root Side
- TT2_ZF_Center (Cross Section)
- TT2_ZF_Face Side
- TT3_ZF_Root Side
- TT3_ZF_Center (Cross Section)
- TT3_ZF_Face Side
- TT4_ZF_Root Side
- TT4_ZF_Center (Cross Section)
- TT4_ZF_Face Side

X-axis: MB; TT1 - no Purge Gas; TT11 - Purge Ar + 25% CO_2 at 6 L/min; TT12 - Purge Ar + 25% CO_2 at 12L/min; TT13 - Purge Ar + 25% CO_2 at 18L/min — **Samples**

Y-axis: Ferrite Content (%)

(e)

Legend:
- MB_Root Side
- MB_Center (Cross Section)
- MB_Face Side
- TT1_ZF_Root Side
- TT1_ZF_Center (Cross Section)
- TT1_ZF_Face Side
- TT2_ZF_Root Side
- TT2_ZF_Center (Cross Section)
- TT2_ZF_Face Side
- TT3_ZF_Root Side
- TT3_ZF_Center (Cross Section)
- TT3_ZF_Face Side
- TT4_ZF_Root Side
- TT4_ZF_Center (Cross Section)
- TT4_ZF_Face Side

X-axis: MB; TT1 - no Purge Gas; TT14 - Purge Ar + 2% O_2 at 6 L/min; TT15 - Purge Ar + 2% O_2 at 12L/min; TT16 - Purge Ar + 2% O_2 at 18L/min — **Samples**

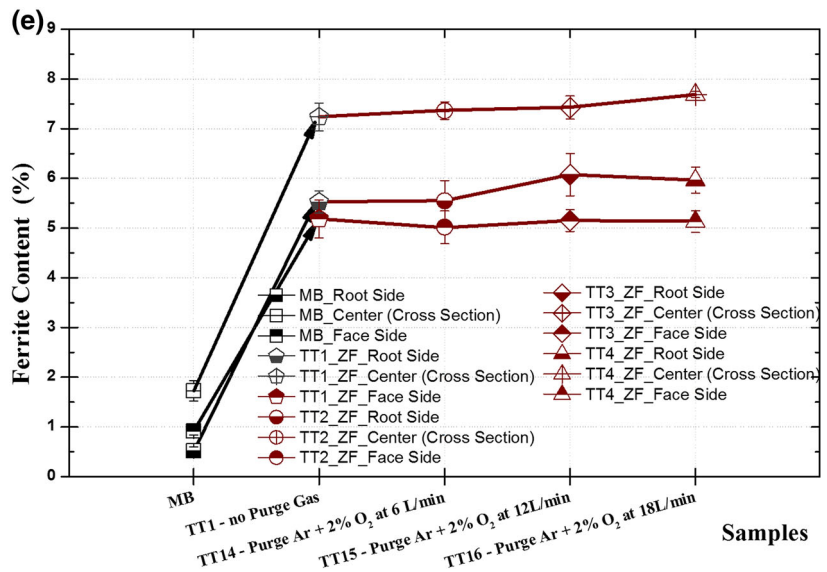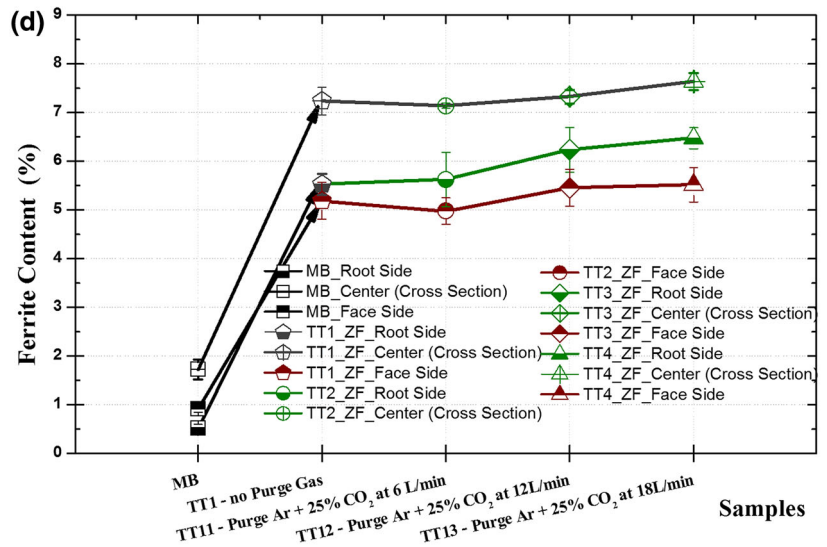Y-axis: Ferrite Content (%)

Table 4 Ferrite content (%) evaluated in the center line in the FZ (root–face)

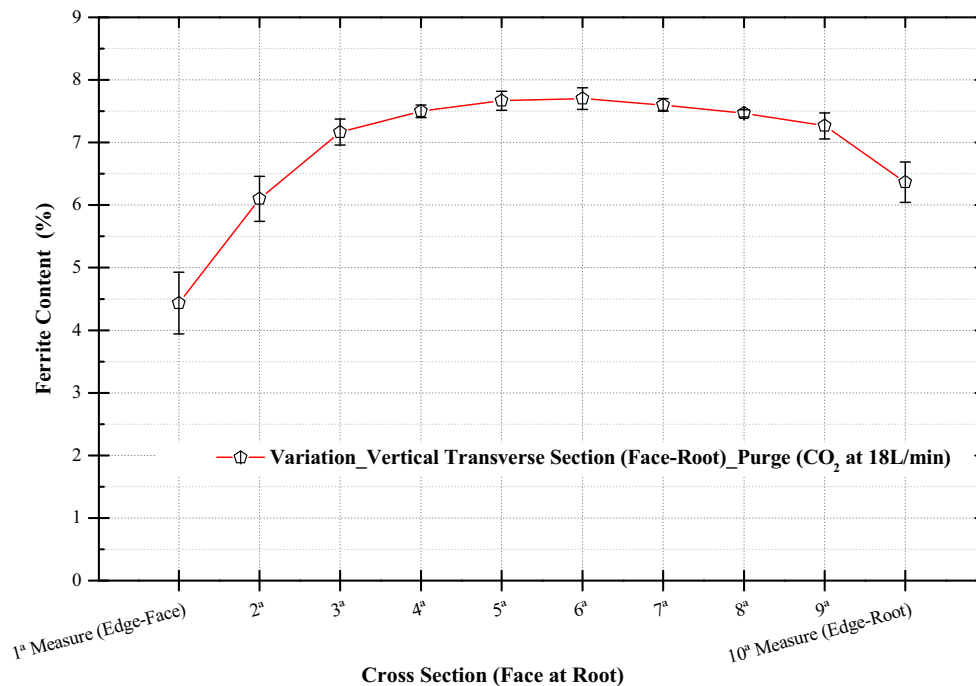| Cross-vertical positioning (face against root)	Medium values Purge (CO_2 at 18 L/min)	SD
1st measure (edge–face)	4.43	0.49
2nd	6.10	0.36
3rd	7.17	0.21
4th	7.50	0.10
5th	7.67	0.15
6th	7.70	0.17
7th	7.60	0.10
8th	7.47	0.06
9th	7.27	0.21
10th measure (edge–root)	6.37	0.32

SD Standard deviation

Fig. 16 Behavior of the ferrite content in the FZ in the transverse-vertical position in line in the center of the root: TT4—CO_2 purge at 18 L/min

significant as the flow rate was increased, with the exception of the N_2 gas.

References

1. Vashishtha H, Taiwade RV, Sharma S, Patil AP (2017) Effect of welding processes on microstructural and mechanical properties of dissimilar weldments between conventional austenitic and high nitrogen austenitic stainless steels. J Manuf Process 25:49–59
2. Fletcher M (2016) Gas purging optimizes root welds. Weld J 85(12):38–40
3. Taban E, Kaluc E, Aykan TS (2014) Effect of the purging gas on properties of 304H GTA welds. Weld J 93(4):124S–130S
4. Madhusudhan Reddy G, Mohandas T, Sambasiva Rao A, Satyanarayana VV (2005) Influence of welding processes on microstructure and mechanical properties of dissimilar austenitic–ferritic stainless steel welds. Mater Manuf Process 20:147–173
5. Ebrahimi Ahmad Nejad, Bani Mostafa Arab N, Hoseinpour Gollo M (2016) Thermal analysis of laser beam welding of nickel-based super alloy Inconel 625 to AISI 316L, using Gaussian optics theory in keyhole. J Braz Soc Mech Sci Eng 38:1199–1206
6. Galdino LG (2014) Influence of purge gas in the root welds formation in stainless steel AISI 304 tube. PhD Thesis, Federal University of Uberlandia, Uberlândia, Brazil
7. Agrawal BP, Chauhan Ankit Kumar, Kumar Ravindra, Anant Ramkishor, Kumar Sudhir (2017) GTA pulsed current welding of thin sheets of SS304 producing superior quality of joint at high welding speed. J Braz Soc Mech Sci Eng 39:4667–4975
8. Chen X, Li J, Cheng X, He B, Wang H, Huang Z (2017) Microstructure and mechanical properties of the austenitic stainless steel 316L manufactured by gas metal arc additive manufacturing. Mater Sci Eng A 703:567–577
9. Ma D, Zhanga Z, Li Y (2015) Investigation of gas purging process in pipeline by numerical method. Process Saf Environ Prot 94:274–284
10. Kah P, Martikainen J (2013) Influence of shielding gases in the welding of metals. Int J Adv Manuf Technol 64:1411–1421
11. Wang Z, Palmer TA, Beese AM (2016) Effect of processing parameters on microstructure and tensile properties of austenitic stainless steel 304L made by directed energy deposition additive manufacturing. Acta Mater 110:226–235
12. Westin EM, Olsson COA, Hertzman S (2008) Weld oxide formation on lean duplex stainless steel. Corros Sci 50:2620–2634
13. Zhang Z, Jing H, Xua L, Hana Y, Zhaoa L, Zhou C (2017) Effects of nitrogen in shielding gas on microstructure evolution and localized corrosion behavior of duplex stainless steel welding joint. Appl Surf Sci 404:110–128
14. Paulraj P, Garg R (2016) Effect of welding parameters on pitting behavior of GTAW of DSS and super DSS weldments. Eng Sci Technol Int J 19:1076–1083
15. Kotecki DJ, Siewert TA (1992) WRC-1992 constitution diagram for stainless steel weld metals: a modification of the WRC-1988 diagram. Weld J 71(5):171S–178S
16. American Welding Society. AWS-D10.4 (1986) Recommended practices for welding austenitic chromium-nickel stainless steel piping and tubing. American National Standards Institute, USA
17. American Welding Society. AWS A3.0M/A3.0. (2010) Standard welding terms and definitions, 12th ed. American National Standards Institute, USA
18. ASM International Handbook (2004) Metallography and microstructures. Metals Handb 9:589–1667

19. ASTM-E407 – 07 (2011) Standard practice for microteaching metals and alloys. American Society for testing and materials, USA

20. Modenesi PJ, Apolinario ER, Pereira LM (2000) TIG welding with single-component fluxes. J Mater Process Tech 99:260–265

21. Inoue H, Koseki T, Ohkita S, Fuji M (2000) Formation mechanism of vermicular and lacy ferrite in austenitic stainless steel weld metals. Sci Technol Weld Join 5:385–396

22. Liao MT, Chen WJ (1998) The effect of shielding-gas compositions on the microstructure and mechanical properties of stainless steel weldments. Mater Chem Phys 55:145–151

23. Filho DF, Ferraresi VA, Scotti A (2010) Shielding gas influence on the ferritic stainless steel weldability. Proc Inst Mech Eng Part B J Eng Manuf 224:951–961